Published in Metall. Mater. Trans. A, 2004, vol. 35, 771-83

EFFECT OF BROACHING ON HIGH TEMPERATURE FATIGUE BEHAVIOUR IN NOTCHED SPECIMENS OF INCONEL 718

T. Connolley, M. J. Starink & P. A. S. Reed *
Materials Research Group, School of Engineering Sciences
University of Southampton, Highfield, Southampton, SO17 1BJ, United Kingdom

ABSTRACT

Notches were machined in specimens of Inconel 718 by a broaching process, where differing broaching runs led to differing extents of sub-surface deformation and surface roughness. Fatigue tests were carried out at 600˚C with a trapezoidal loading waveform at 0.25Hz. The broaching process that led to the more severe sub-surface deformation (but lower surface roughness) showed the worst fatigue performance. Analysis of total strain amplitude in the notch root with the aid of an elasto-plastic finite element model, showed that the work-hardening related to the subsurface deformation caused by the different broaching can account for the difference in fatigue lives. Differences in initiation and growth behaviour were seen for the two broached finishes as well as for broached and subsequently polished samples. These differences are discussed in terms of a change in crack growth initiation and growth mechanisms due to the presence of the work hardened layer.

I. INTRODUCTION

In the broaching process, a cutting tool with multiple shaped teeth is drawn through a hole or over a surface to remove material by axial cutting [1]. Figure 1 shows a schematic diagram of a broaching tool and its application in the machining of a U-notch specimen of the type used in this study (Figure 2). With appropriate tool design, complex profiles can be machined with the single pass of a tool. In gas turbines, the blades are usually attached to the rims of turbine discs using a fir-tree root fixing and the complex notch geometry in the rim is commonly produced by broaching. The stress concentration effect of the notch means that fatigue initiation in this region is more likely. One type of in-service damage to turbine discs that must therefore be considered is low cycle fatigue (LCF) cracking in the fir tree root fixtures.

For the present work the Inconel® 718 (IN718) nickel based superalloy was chosen due to its current and projected widespread use for gas turbine discs. The majority of published LCF studies on this alloy have concentrated on the effects of temperature and environment on long crack propagation rates. This has included studies of mechanisms of grain boundary oxidation and its influence on fatigue crack propagation [2,3,4]. Dwell times at maximum or minimum

load were generally found to increase crack propagation rates, with the dwell permitting the time-dependent oxide embrittlement of grain boundaries [5,67891011]. Most of these studies were on long cracks using CT specimens, but the hold time effect has also been observed for pre-initiated cracks in U-notch specimens tested in bending [12].

Compared to the wealth of knowledge on IN718 obtained from laboratory long crack fatigue testing, relatively little is known about high temperature crack initiation and short crack growth in this alloy. Various studies on a range of superalloys have identified high temperature crack initiation at slip bands [13,14], inclusions [15], pre-cracked carbide particles [16] and preferentially oxidised carbides [17,181920]. Volume expansion of oxidising primary carbides was identified as a mechanism of environmentally assisted crack propagation in notch-rupture tests on IN718 [21]. The role of oxidised primary carbides in fatigue crack initiation has also been studied [22,23,24,25].

Additionally, there is an interest in understanding crack behaviour in notched geometries like the fir-tree root fixings in a turbine disc rim. The natural initiation and growth of short cracks in U-notch IN718 specimens has been studied at 600^{o}C in air and reported in detail elsewhere by the authors [25]. Fatigue tests were conducted under load control using a 1-1-1-1 trapezoidal waveform, on specimens with as-broached and polished U-notches. Multi-site crack initiation occurred in the notch root. Many of the cracks initiated at bulge-like features formed by volume expansion of oxidising (Nb,Ti)C particles. In unstressed samples, oxidation of (Nb,Ti)C particles occurred readily, producing characteristic surface eruptions. Scanning electron microscopy on metallographic sections revealed some sub-surface (Nb,Ti)C oxidation and localised matrix deformation around oxidised particles. A mechanism for crack initiation by sub-surface carbide expansion during oxidation was proposed. Surface short crack growth rates in the notch root of polished specimens were measured using an acetate replica technique. Observed short crack growth rates were approximately constant across a wide range of crack lengths. However, there was a transition to rapid, accelerating crack growth once cracks reached several hundred microns in length. This rapid propagation in the latter stages of the fatigue life was assisted by crack coalescence. Polishing the U-notch to remove broaching marks resulted in a pronounced increase in fatigue life.

The purpose of this paper is to compare fatigue crack behaviour in two batches of IN718 specimens with broached U-notches, where separate broaching runs led to different initial notch roughness and levels of sub-surface deformation. This includes study of the natural initiation and propagation characteristics of short cracks in broached notched IN718 specimens at 600^{o}C in air (conditions similar to those experienced in the fir tree root fixings of a gas turbine disc). Crack initiation and growth in the polished notch root (thus removing

any surface roughness effects) has also been compared for the two batches of specimens.

II MATERIAL & SPECIMEN CHARACTERISATION

Two batches of single edge U-notch specimens, labelled Batch A and Batch B, were extracted from two IN718 turbine disc forgings produced from the same cast of material. Each forging was solution treated at 955^{o}C for 1 hour followed by an air cool, then aged at 720^{o}C for 8 hours, cooled at 50^{o}C/h to 620^{o}C, aged at 650^{o}C for a further 8 hours, finishing with an air cool. The composition of the disc material was B – 0.003wt%, C – 0.031 wt%, N – 0.006 wt%, O – 0.00006wt%, Mg- 0.002 wt%, Al – 0.46wt%, Si – 0.08 wt%, P – 0.01wt%, S – 0.0004Wt%, Ti – 1.02 wt%, Cr – 18.0wt%, Mn – 0.06 wt%, Fe – 18.6wt%, Co – 0.43 wt%, - bal. Ni. The U-notch specimen geometry is shown in Figure 2. The dimensions of the U-notch were chosen to give a stress concentration factor similar to a blade fir tree root fixing in a turbine disc rim. Finite element (FE) modelling of the specimen predicted an elastic stress concentration factor of 2.08. Notches were machined in each batch using a broaching process similar to that used for machining fir tree root fixings in production discs. The broaching process produced long machining marks parallel to the notch axis. A Talysurf instrument was used to obtain the following measures of surface roughness in the notch roots:

R_a = average deviation from the mean surface.
R_v = maximum valley depth below the mean surface detected in a measurement run.

Three measurement runs (t1-t3) were made perpendicular to the notch axis per specimen, spaced at 5mm intervals and acquired using a data length of 1.04mm and a cut-off length of 0.08mm - the longest data length possible without risk of damage to the Talysurf stylus. Metallographic sections were taken to assess any microstructural changes that may have occurred as a result of the broaching process. General microsections were also taken to compare the microstructure in the two specimen batches. Metallographic samples for optical microscopy and SEM examination were prepared using standard techniques. Specimens were etched using Nimonic etch (10 ml HNO_3, 50 ml HCl, 40 ml H_2O & 2.5g $CuCl_2$). Optical microscopy combined with image analysis was used to determine grain size and primary carbide volume fraction. A JEOL JSM 6400 scanning electron microscope (SEM) was used for fractography and further metallography. The identity of phases was confirmed by energy-dispersive X-ray spectrometry (EDS). Microhardness measurements were performed on cross-sections to establish if surface layers exhibited signs of work hardening. An indent small enough to be entirely within limited deformation layers, but with a test mass large enough to give a true representation of hardness was required. In each case twenty near-surface measurements were performed using a test mass of 200g. Indents were located 20 μm below the notch surface.

III FATIGUE TEST METHODS

Three-point bend fatigue tests were conducted in air at 600^{o}C under load control, using a 1-1-1-1 trapezoidal waveform (Figure 3). Specimens were heated inside a high temperature chamber mounted on an Instron 8501 servo-hydraulic testing frame. The temperature was monitored and controlled via an R-type thermocouple attached to the front face of each specimen. For all tests the recorded temperature was within +/- 2^{o}C of the target temperature. Tests were performed at a load ratio R = 0.1 and nominal maximum stresses σ_{max} from 750 MPa to 1000 MPa were employed. Applied loads were calculated to give the desired nominal value of σ_{max} in the net specimen cross section (i.e. ignoring the stress concentrating effect of the notch). Elastic-plastic FE modelling of the U-notch specimen was performed to predict the strain range in the notch root for the different nominal applied stress levels. In terms of the individual total strain components, the equivalent strain range was calculated as follows:

$$\Delta\varepsilon_{eq} = \frac{\sqrt{2}}{3}\left[\left(\Delta\varepsilon_{xx} - \Delta\varepsilon_{yy}\right)^2 + \left(\Delta\varepsilon_{yy} - \Delta\varepsilon_{zz}\right)^2 + \left(\Delta\varepsilon_{zz} - \Delta\varepsilon_{xx}\right)^2 + \frac{3}{2}\left((\Delta\gamma_{xy})^2 + (\Delta\gamma_{yz})^2 + (\Delta\gamma_{xz})^2\right)\right]^{\frac{1}{2}} \quad [1]$$

Each strain component included elastic and plastic contributions. The strain amplitude is given by:

$$\varepsilon_{amp} = \frac{\Delta\varepsilon_{eq}}{2} \quad [2]$$

The majority of tests were performed on specimens with notches in the as-broached condition, to represent the surface finish present in a production turbine disc. These tests were run to failure, then examined in an SEM to identify the crack initiation sites. A second set of tests was performed on specimens with notch surfaces mechanically polished to a 1 μm diamond finish. To minimise notch enlargement, specimens were secured in a specially-designed jig and polished using soft 4mm diameter x 8mm long cylindrical dental felts mounted in a pillar drill. Selected polished notch tests were interrupted in order to take cellulose acetate replicas from the notch root.

IV RESULTS

A. U-notch Surface Roughness and Microstructure Comparison

Mean R_a and R_v data for Batch A and Batch B are given in Table I. Batch A data are the averages from 15 specimens. Batch B data are the averages from 22 specimens. The polished specimen data are from a Batch B specimen that had received the standard polishing

procedure, where care was taken to use low polishing forces to prevent smearing or residual stress generation, specimens were inspected under an optical microscope and in an SEM after polishing. The authors consider any differences in surface roughness between polished specimens from Batch A or B to be minimal. Maximum R_v values are also listed, to give an indication of the maximum broaching mark depth in each batch. The data show that the notches in Batch B specimens were rougher than those in Batch A. This can be seen in the plot of R_a values for individual specimens displayed in Figure 4. Polishing of the U-notches produced a large reduction in surface roughness.

Table I: Mean surface roughness data for as-broached notch surfaces

	Batch A	**Batch B**	**Polished Specimen**
Mean R_a (μm)	0.1607 (0.0202)	0.4011 (0.0803)	0.0053 (0.0004)
Mean R_v (μm)	0.7960 (0.1567)	1.7574 (0.4369)	0.0258 (0.0086)
Max. R_v (μm)	2.1582	3.1157	0.0357

Standard deviations are given in brackets

Metallographic sections through the notches of as-broached specimens (Figure 5) revealed a difference in the sub-surface microstructure of the notch between Batch A and Batch B. In Batch A, a sub-surface layer was observed which extended all the way round the surface of the U-notch and had the appearance of a zone of heavy localised deformation (Figure 5a). The thickness of the layer was between 10-16 μm in the notch root and up to 40 μm on the notch sides. No deformation layer was observed on the other machined surfaces of the Batch A specimens, only the broached notch surface. In Batch B, a deformation layer was not observed in the broached notch (Figure 5b) or on the other machined surfaces. The deformation layer was still present in Batch A specimens after U-notch polishing. Its apparent depth in the notch root was reduced to approximately 7-10 μm. Away from the notched region both batches had a non-equiaxed grain structure with larger elongated grains (diameter approximately 20-70 μm) surrounded by extensive regions of small, more equiaxed grains (diameter approximately 5-10 μm). The larger grains were elongated in the tangential and radial directions, as would be expected for forged discs. Table II gives the mean linear intercept grain sizes in the three disc forging directions, showing no significant difference in grain size between Batches A and B.

Table II: Mean linear intercept grain sizes, disc material.

	Batch A		Batch B	
Direction	**Mean Linear Intercept (μm)**	**Standard Deviation* (μm)**	**Mean Linear Intercept (μm)**	**Standard Deviation* (μm)**
Tangential	10.8	1.4	9.6	0.6
Radial	10.8	0.4	11.5	0.8
Axial	6.3	0.6	6.7	0.8

*Note the standard deviation is between the different areas assessed.

Grain boundaries were decorated with particles of various morphologies, which EDS revealed to be the δ (Ni_3Nb) phase. Other phases observed using optical microscopy and SEM were primary carbides and nitrides. The combined area fraction of primary carbides and nitrides was determined by image analysis on polished micro sections. The results were 0.37%. for Batch A and 0.33% for Batch B, with very similar size distributions exhibited for both batches. It has been shown [26] that the amount of carbides and nitrides is directly determined by the C and N content of the alloys, and that the measured volume fraction of carbides and nitrides is consistent with the C and N content of the present IN718 alloy.

Microhardness indents on a Batch A notch microsection were located in the deformation layer on the notch sides. These were compared with measurements made on bulk material several millimetres below the surface, and with measurements made in similar locations on a Batch B specimen. The hardness data (Table III) revealed differences in hardness on the surface layers between the batches. It is noted that if we assume a Gaussian distribution of hardness on the measured locations, the limit of 95% confidence in measured average is $2\sigma_D/\sqrt{N}$, with N the number of hardness indentations made (N=20). This means confidence limits are in the range of 4 to 10 and the differences in average hardness are clearly significant. The mean microhardness in the deformed surface layer of the Batch A specimen was approximately 15% higher than that for the bulk material, indicating that the material had been work hardened by the broaching process. This may be an underestimate, due to the effect on hardness readings of reduced constraint near the specimen surface. No evidence of work

hardening was found in the Batch B specimen. The apparently softer Batch B near-surface hardness relative to the bulk value was probably due to reduced constraint near the specimen surface.

Table III: Vickers Microhardness Results

	Batch A		**Batch B**	
	Mean Vickers Microhardness	**Standard deviation**	**Mean Vickers Microhardness**	**Standard deviation**
Near surface	454	23	371	15
Bulk material	394	8	391	9

B. Fatigue Lives

Fatigue results for the as-broached conditions in each batch are displayed as stress-life and strain-life curves in Figure 6 (a) & (b). In Figure 6 (b), lifetimes are plotted against the strain amplitude predicted by Equations 1 and 2. The strain-life data for each batch has been fitted to the Coffin-Manson relationship :

$$\frac{\Delta\varepsilon}{2} = \left(\frac{\sigma_f'}{E}\right)(2N_f)^{\lambda_1} + \varepsilon_f'(2N_f)^{\lambda_2} \qquad [3]$$

where:
$\Delta\varepsilon$ = strain range
σ_f' = fatigue strength coefficient (≈ the uniaxial true fracture stress)
E = elastic modulus
N_f = number of cycles to failure
ε_f' = fatigue ductility coefficient (material-dependent)
λ_1, λ_2 = material-dependent constants.

The parameters of the fitted curves for each batch are given in Table IV. The fit is an empirical one since σ_f', ε_f' and λ_2 are all allowed to vary, but the raw data and the resulting fits do indicate a difference in material fatigue strength/ductility between Batches A and B

It is apparent in Figure 6 that the Batch B exhibited longer fatigue lives than Batch A when tested under the same test conditions. In Figure 7, the fatigue lifetimes of the polished notch roots in both batches can be compared with the performance of the as-broached notch roots. Uninterrupted as well as interrupted polished tests are compared. For uninterrupted tests on

Batch A specimens, polished notches produced longer lifetimes to fracture than as-broached notches under the same test conditions. The beneficial effect of notch polishing was also observed for Batch B specimens tested at σ_{max} = 885 MPa, However, a Batch B polished notch test performed at σ_{max} = 790 MPa had a shorter life than as-broached Batch B specimens. Fractographic examination of this test showed that a crack had initiated at a sub-surface (Ti,Nb)N particle.

Table IV Coffin-Manson fit parameters

	Batch A	Batch B	Comments
E (MPa)	1.68×10^5	1.68×10^5	Held constant
σ_f' (MPa)	580	658	Allowed to vary in fit
λ_1	-0.01	-0.01	Held constant
ε_f'	0.339702	0.445076	Allowed to vary in fit
λ_2	-0.71371	-0.74398	Allowed to vary in fit

C. Initiation behaviour

After fracture, the as-broached specimens were examined in an SEM to characterise the crack initiation sites. Multi-site crack initiation occurred in the notch root. Several types of crack initiation site in air were identified in the two batches:

(i) Bulge-like features associated with the oxidation of sub-surface primary carbides (Figure 8a)
(ii) Surface eruptions formed by the oxidation of primary carbides (Figure 8b)
(iii) Initiation at (Ti,Nb)N particles (Figure 8c)
(ii) Small bulge-like features NOT associated with the oxidation of sub-surface primary carbides (Figure 8d)
(v) Sites with no obvious surface eruption, bulge or nitride particle.

Additional information about the crack initiation process in air was obtained from the interrupted tests on polished specimens. Examination of surface replicas taken during the interrupted tests showed that cracks began to initiate within the first 10% of the overall fatigue life. The evolution of the number of cracks present in the notch root as tests progressed is shown in Figure 9 for σ_{max} = 750 MPa and σ_{max} = 790 MPa in Batch A. For both tests, the majority of cracks initiated at bulge-like features, with the remainder starting at surface eruptions or at sites with no discernable eruption or bulge (termed intrinsic initiation). A common feature in both tests was an incubation period at the beginning of the test in which

no cracks were observed. After the initial incubation period, the number of cracks increased at a steady rate. The initiation rate then decreased. Eventually, major coalescence of cracks led to rapid reduction in the number of individual cracks observed in the notch root.

For as-broached specimens, it was observed that the total number of initiation sites per specimen was much lower for Batch B than Batch A tested under the same conditions. It was also observed that unlike Batch A, the most numerous crack initiation sites were not oxidised primary carbides (eruptions or bulge-like sites). Instead, the most numerous sites were the sites with no apparent feature on them. Sometimes, small bulge-like features were observed, but they were not associated with sub-surface (Nb,Ti)C particles. EDS analysis of these bulges showed there was some slight enrichment in Nb relative to the matrix, but not the very high enrichment in Nb indicating the presence of an (Nb,Ti)C particle. Examples of these bulges without associated particles are shown in Figure 8d. These small bulges were not evident elsewhere on the notch surface, unlike the prominent bulges associated with (Nb,Ti)C carbide particles observed on Batch A specimens. Where an (Nb,Ti)C particle was present at an initiation site in a Batch B specimen, this was easily confirmed by the high Nb signal detected using EDS. Occasionally, initiation at (Ti,Nb)N particles was observed, as shown in Figure 8(c). The (Ti,Nb)N particles in the material were known to be Ti rich and this was used to confirm the identity of the particles at initiation sites.

The evolution of the number of cracks present in the notch root as tests progressed is shown in Figure 10 for 2 tests carried out at σ_{max} = 885 MPa in Batch B. For the test represented in Figure 10(a) the dominant crack initiated at a surface eruption and was first observed after 1000 cycles. This was the only crack to grow significantly. Most of the other cracks which initiated did so late in the fatigue life ahead of the main crack tip and in the residual ligaments. In Figure 10(b) the dominant and only significant crack was first observed after 1000 cycles at a (Ti,Nb)N particle, and again the majority of cracks initiated late in the fatigue life ahead of the main crack tips of the dominant crack. This was different from the behaviour seen in Batch A at σ_{max} = 750 MPa and 790 MPa where cracks initiated and grew from several sites and later coalesced to form the final dominant crack.

The difference in initiation characteristics between the Batch A and Batch B tests can be seen in Figure 11(a) and (b), where the total number of cracks observed is plotted against number of cycles (a) or percentage of life (b). In all four tests, crack initiation rates were low at first, up to 5000 cycles. The Batch A tests at σ_{max} = 750 MPa and 790 MPa then exhibited crack initiation at a fairly constant rate before reaching a plateau, with a decrease in crack numbers at the end of the life due to coalescence. However, the two Batch B σ_{max} = 885 MPa tests showed very rapid crack initiation with no plateau and no significant crack coalescence,

followed shortly by specimen fracture. Comparing crack initiation behaviour plotted against percentage of fatigue life, the difference in initiation behaviour between the lower stress levels (σ_{max} = 750 & 790 MPa) and σ_{max} = 885 MPa is also apparent. The lives of the tests at 750 and 790 MPa therefore appeared to be initiation dominated, whereas the tests at 885 MPa were propagation dominated.

D. Crack propagation paths

Striking differences were observed in the propagation characteristics of cracks between the two batches. In Batch A, extremely straight, apparently transgranular crack growth was observed for all cracks, except where the tips underwent local deflection during crack-crack interactions. An example of this remarkably straight crack growth can be seen in Figure 12, where an acetate replica of a crack initiating from a bulge can be seen. The fatigue fracture surface produced by such crack growth can be seen in Figure 13, showing a transition from very flat transgranular fracture to mixed transgranular/intergranular fracture as the crack propagates into the depth of the specimen, again a sub-surface bulge associated with an enlarged particle ((Nb,Ti)C) can be seen at the initiation site. In the batch B specimens more crack deflections were observed (most easily seen in the polished specimens). Figure 13 shows an example of such a crack, which in this case has initiated from a TiN particle, the crack path exhibits many more deflections with apparent mixed transgranular/intergranular propagation, the crack path appears to become more intergranular as the crack becomes longer. There is clear evidence of slip band formation in adjacent grains, which was not observed in the polished tests carried out in Batch A.

Fatigue life results showed that polished specimens usually had longer lifetimes than as-broached specimens tested under the same conditions. Since the broaching marks were parallel to the notch root and hence the direction of surface crack propagation, it was possible that the broaching marks were accelerating crack initiation and/or crack propagation, resulting in shorter fatigue lives than polished specimens. In the Batch A tests, the cracks observed were straight and parallel to the notch axis on both as-broached and polished specimens. Hence it was not possible to determine conclusively if the broaching marks affected crack propagation. However, for the Batch B tests, there was some evidence that the broaching marks were influencing crack propagation. SEM fractography was performed on uninterrupted run to fracture tests performed under the same conditions, comparing an as-broached and a polished notch. Comparisons of the surface crack path in the notch root near the main crack initiation site are shown in Figure 15. In the as-broached notch, the surface crack path was essentially straight and parallel to the broaching marks, whereas in the polished notch the crack path deviated along slip bands or grain boundaries.

V DISCUSSION

Both discs were produced consecutively from the same cast of material using the same forging and heat treatment process, so one would expect a similar microstructure to result. This is borne out by the results of metallography on the two batches of specimens, showing them to have similar grain sizes, similar area fractions of primary carbides and nitrides and similar size distributions of primary carbides and nitrides. However, two differences between the as-received batches of U-notch specimens were surface roughness and the presence of what appeared to be a work-hardened deformation layer in the notch surface of Batch A specimens. Both these observations point to differences in the broaching process used to machine the U-notches. It is believed that the deformation layer in Batch A specimens arose from use of a blunt tool, causing local deformation of the material rather than cutting it cleanly. These two differences, and especially the work hardened layer, are thought to be the cause of the different crack initiation and crack growth behaviour of the two batches, as will be discussed below.

Previous work by the authors on Batch A specimens [25] demonstrated that primary carbides at or close to the surface of IN718 oxidised at elevated temperatures, and there was a substantial volume expansion associated with oxidation. This was observed in unstressed specimens and U-notch fatigue specimens exposed at 550^{o}C and 600^{o}C in air. The Batch A U-notch tests in particular exhibited a link between primary carbide oxidation, localised matrix deformation and fatigue crack initiation. Intense planar slip in Batch B specimens (the specimens without a work hardened layer) was evident from the slip bands visible on polished U-notch surfaces at σ_{max} = 790 MPa and σ_{max} = 885 MPa. Compared to Batch A specimens, a greater proportion of fatigue cracks initiated intrinsically, rather than at oxidised primary carbides. These observations are thought to be linked; if intense slip bands develop in a material, then these can lead to crack initiation in a variety of ways, including slip-step formation producing local notches on the fatigue surface or at stress concentrations arising from slip band interaction with grain boundaries or carbides/nitrides. Formation of intense slip bands and crack initiation along them is promoted by cyclic softening, with dislocations preferentially gliding along the softer band rather than in the harder surrounding regions [27,28]. IN718 is sensitive to the environment at elevated temperatures and grain boundary embrittlement by oxidation can occur [7,29,8]. Impingement of slip bands on grain boundaries produces local stress concentrations at the boundary. The slip bands can also act as fast diffusion paths for diffusion of oxygen, accelerating grain boundary oxidation. Hence, stress concentrations at a grain boundary combined with grain boundary embrittlement may initiate cracks. In the case of the U-notch specimens, crack initiation appeared to be predominantly transgranular, so grain boundary embrittlement was not a major mechanism of crack initiation in this case. However, some intergranular crack propagation was observed on fracture surfaces, so the

environment was affecting crack propagation paths.

A few bulges were observed at Batch B initiation sites which were not associated with oxidised primary carbides. These features may have been an artefact of the broaching process, or small protrusions of material - possible evidence of intense slip band formation and were of a similar scale to slip band extrusions observed elsewhere []. Note that in as-broached specimens, the roughness of the U-notch masked the appearance of slip bands on the notch surface. Protrusions where slip bands intersect a free surface may act as crack initiators due to the local stress concentrating effect of the step formed. Some intrinsic initiation was observed in Batch A specimens as well as in the Batch B specimens, though intense slip bands were not seen in the polished notch roots of Batch A specimens. However, there may still have been crack initiation in the Batch A notch roots along favourably oriented slip lines, and machining marks on as-broached specimens could also have acted as crack initiators.

The bulges above oxidised carbides seen at crack initiation sites in the Batch A U-notch fatigue tests are evidence for extensive plastic deformation in the matrix around oxidising sub-surface primary carbides, as predicted by the misfit calculations in previous work [25]. For a mechanism of fatigue crack initiation in the Batch A U-notch specimens, it is proposed that the misfit strains due to carbide oxidation were superimposed on the elastic-plastic stress-strain field due to external loading. This created local strains high enough to cause fracture of the matrix in the vicinity of an oxidising particle, hence initiating a fatigue crack. The plastic deformation in the notch root and the formation of slip bands may have promoted stress-assisted oxygen diffusion, causing more rapid oxidation of the sub-surface primary carbides than that observed for unstressed thermal exposure specimens. Once a crack initiated, the crack itself provided another fast oxygen diffusion route to a sub-surface particle. The surface cracks observed experimentally at oxidised sub-surface carbides were very sharp, probably resulting in a high stress intensity at the crack tip which drove further propagation.

Matrix deformation was seen around some surface eruptions formed by oxidised (Nb,Ti)C carbide particles. It was originally thought that initiation at these surface oxide eruptions might be due to the micro-notch effect of a cavity beneath the erupted particle. However, the observation of matrix deformation associated with some surface eruptions in thermal exposure specimens and on the U-notch fatigue specimens suggests that it was the additional matrix strain caused by expansion mismatch which assisted crack initiation. Matrix deformation, combined with plastic strain accumulation from the fatigue loading could have caused initiation from those surface eruptions which produced sufficient misfit strains in the matrix. Initiation from surface eruptions was observed in Batch A and Batch B specimens, though many surface eruptions in both batches of material did not initiate cracks, so that only

those eruptions which produced high enough misfit strains acted as crack initiators.

The high incidence of bulges at crack initiation sites in Batch A specimens suggests that expansion of oxidising sub-surface primary carbides was a significant mechanism of fatigue crack initiation in the notch root. Certainly for Batch A specimens, it was the oxidised sub-surface carbides, rather than oxide eruptions in general, that were the more numerous type of crack initiation site in U-notch specimens tested in air. This was not the case for Batch B specimens, in which initiation at oxidised sub-surface carbides was infrequent. The difference in crack initiation behaviour between the two batches of specimens when tested under the same conditions must arise from the different roughness of the broached U-notch surfaces and/or the local microstructure in the notch root.

Surface roughness will affect crack initiation behaviour. Generally, rougher surfaces result in earlier crack initiation and shorter fatigue lives, due to the local stress concentration effect of surface features like scratches and machining marks. In a study by Andrews et al. [30] on two microstructural variants of IN718, it was found that machining marks, rather than microstructure, were controlling crack initiation life in double edge notch specimens at 650^{o}C. In this study, if surface roughness was the critical factor, Batch B would be expected to exhibit worse fatigue performance than Batch A. However, the as-broached Batch B specimens had longer lives, as shown in Figure 6, and generally fewer initiation sites than Batch A specimens tested under the same conditions. For polished Batch B specimens, the total number of initiation sites was also lower than in Batch A. Surface roughness alone does explain the difference in initiation behaviour between Batch A and Batch B.

The other difference between the notches in Batch A and Batch B was the presence of a deformation layer in the Batch A samples. This was up to 40 μm thick on the notch sides and approximately 10-16 μm thick in the notch root. The layer was not observed in Batch B specimens. Vickers microhardness measurements indicated that the surface deformation layer was approximately 15% harder than the bulk material in Batch A specimens. Cahoon et al. [31] related yield stress to hardness using the formula:

$$\sigma_y = 9.81\left(\frac{H_v}{3}\right)(Q)^{n)} \qquad [4]$$

where:
σ_y = yield stress in MPa
H_v = Vickers hardness
Q = a constant
n = work hardening exponent

From equation 4 it follows that providing *n* is constant, for a 15% increase in hardness a 15% increase in yield stress is predicted. This higher localised yield stress may have influenced crack initiation behaviour. Considering a purely continuum approach, it is possible to estimate how the higher local yield stress affected the local strain amplitude, and hence the strain-life characteristics of the Batch A specimens. Ideally, this should have been done by modifying the FE model to take into account a higher local yield stress at the notch surface, but this was not possible using the existing mesh or the user-defined constitutive model. Instead, a simplified approach was adopted, using the existing FE model outputs of elastic and plastic strain components at the notch root centre. A 15% increase in yield stress will increase the elastic strain before yielding occurs by the same factor, so the elastic components of strain in the notch root at σ_{max} were increased by a factor of 15% to reflect this. It was not possible to establish the effect of an increased yield stress on plastic strain components, so these were assumed to be unchanged. This assumption was considered reasonable, since most of the reversible strain in the notch root was due to the elastic contribution. The total strain amplitudes ε_{amp} for Batch A tests were then re-calculated using equation 1 and equation 2. The resulting adjusted strain-life curve for Batch A is compared with the original Batch B results in Figure 16 and the appropriate Coffin-Manson fit data is compared in Table V. With total strain amplitudes adjusted to account for pre-existing cold work hardening in the notch root, the Batch A results now lie close to those obtained for Batch B specimens. Hence, an increased local yield stress and total strain amplitude in the notch root could explain the difference in the strain-life behaviour between Batch A and Batch B specimens, in the present continuum approach. It should be noted that in this analysis we are considering the local area of material in the notch root, and the empirical Coffin-Manson fits to the data are consistent with the broaching in Batch A having a detrimental effect on the fatigue strength/ductility of the material in the notch root. Fatigue life appears to be dominated by initiation/short growth, therefore the condition of the material in the localised area of the notch root is clearly important.

Table V Coffin-Manson fit parameters

	Batch A	Batch B	Batch A (hardened)	Comments
E (MPa)	1.68×10^5	1.68×10^5	1.68×10^5	Held constant
σ_f' (MPa)	580	658	580	Allowed to vary in fit
λ_1	-0.01	-0.01	-0.01	Held constant
ε_f'	0.339702	0.445076	0.010305	Allowed to vary in fit
λ_2	-0.71371	-0.74398	-0.2767	Allowed to vary in fit

In considering a more microstructural explanation of the role of the surface layer, it is noted that the higher yield stress of the work-hardened layer will have led to greater stresses around mis-fitting particles. For example, with a 15% increase in σ_y, the maximum value of the predicted hoop stress calculated from the model presented in Ref. [25] increases from 327 MPa to 376 MPa. For a carbide particle oxidising in the deformation layer of Batch A, these higher misfit stresses combined with the external loading may have enhanced crack initiation and early crack growth. This is consistent with the observation of many cracks initiating at oxidised carbides in Batch A, but only a few in Batch B. An additional effect on crack initiation and propagation in Batch A may have resulted from reduced ductility in the work-hardened layer. In a few cases in Batch B, crack initiation at primary nitride particles was observed. This was probably due to slip band impingement on the particles, producing stress concentrations at the particle-matrix interface which resulted in crack initiation either by cracking of the particle or decohesion of the particle-matrix interface. This mechanism of crack initiation has been observed in other superalloys containing primary carbide and nitride particles, such as Incoloy 908 [32].An interesting experiment to sort out the role of sub-surface oxidation versus surface condition as the primary initiation mechanism would be to impart a compressive stress on the immediate surface layer by shot peening and then perform equivalent fatigue tests.

The quantitative data for the number of crack initiation sites show that there were more initiation sites in Batch A specimens than in Batch B specimens tested under the same conditions. As already discussed, this may be linked to the deformation layer present in Batch A specimens. General observations on interrupted U-notch tests indicated that cracks first initiated within the first 25% of the overall fatigue life. More detailed crack initiation data was obtained from the interrupted replica tests on polished U-notch specimens, as shown in Figure 11 (a) and 11(b). Comparing these plots of number of cracks versus number of cycles, it can be seen that there were differences in initiation kinetics between the Batch A specimens tested at the lower stress levels σ_{max} = 750 MPa or σ_{max} = 790 MPa, and the high stress level Batch B tests at σ_{max} = 885 MPa. For the Batch A tests there was an initial incubation period at the start in which no cracks were observed. The initially slow rate of crack nucleation in both tests is indicative of some form of incubation period necessary for crack initiation. Some of the first cracks observed initiated at bulges due to sub-surface primary carbide oxidation, so the incubation period for initiation is linked to the time required for oxidation of the particles. The time at the test temperature of 600^{o}C was between 2 and 6 hours – a factor of 10 less than the time required for sub-surface oxidation in unstressed thermal exposure samples [25]. This implies a strong effect of fatigue cycling on the kinetics of oxidation, probably caused by enhanced oxygen transport along slip bands. The first particles to oxidise and initiate cracks

may have been those favourably situated for fast oxygen diffusion to the particles, either being close to the surface or on a grain boundary. As already discussed, the deformation layer present in the notch root of Batch A specimens may have promoted faster diffusion. Following the initially slow rate of crack initiation, there was a transition to behaviour in which the number of cracks appearing increased at a steady rate, which was similar in both tests. The factors controlling this rate are thought to be the time required for oxidation of carbides in different parts of the specimen and the time required for accumulation of sufficient cyclic damage in the material to initiate further cracks. The number of primary carbides which are potential crack initiation sites will depend upon the number density of primary carbides in the material, their distribution relative to the notch surface and their distribution relative to preferential oxygen diffusion pathways such as grain boundaries. The local stress-strain environment around potential crack initiation sites will vary, depending on the position of the site in the notch root and shielding by cracks which have already initiated. The number of cracks initiated eventually reached a plateau, which can be attributed to a combination of exhaustion of potential crack initiation sites, reduction in the local strain at initiation sites due to shielding by neighbouring cracks, and crack coalescence.

In Batch B tests the development of crack initiation over time was significantly different from the Batch A tests performed at lower stress levels. Figure 11 shows that few cracks initiated until the latter stages of the fatigue life. As described earlier, the fatigue failure was controlled by initiation and growth of a single crack, with most of the other cracks initiating in the stress-strain field ahead of the tip of the growing crack or in the residual ligaments. One possible cause of the difference between Batch A and Batch B tests was the absence of a work-hardened surface layer in Batch B. This may have reduced the propensity for crack initiation at oxidised carbides compared to Batch A specimens. Another possible reason for reduced crack initiation was the much higher stress level used for Batch B. This led to a shorter fatigue life, allowing less time for sub-surface carbide oxidation and hence limited initiation by an oxidation mis-match strain mechanism. The formation of persistent slip bands was enhanced by the greater strain range in the notch root at σ_{max} = 885 MPa, and the absence of a surface deformation layer may also have promoted persistent slip band formation. This permitted rapid propagation of the dominant surface crack along slip bands or grain boundaries, reducing the potential for crack initiation elsewhere due to shielding by the main crack, except in the high stress regions ahead of the crack tips in the residual ligaments.

One feature that may have affected crack propagation was the presence of broaching marks in the notch roots. The marks were straight and parallel to the notch axis and therefore favourably oriented to influence crack propagation. In Batch A specimens, cracks in the notch root were straight and parallel to the notch axis in both as-broached and polished specimens,

so a conclusive link between broaching marks and crack propagation path was not apparent. In Batch B specimens, a clear difference between microscopic crack paths was apparent when as-broached and polished specimens tested under the same conditions were compared. For an as-broached notch, the surface crack path was essentially straight and parallel to the broaching marks, whereas in a polished notch the crack path deviated along slip bands or grain boundaries, as shown in Figure 15. This difference may help to explain why polished specimens generally had longer fatigue lives than as-broached ones. In as-broached specimens, the broaching marks could have a micro-notch effect, providing a favourable pathway for surface crack growth parallel to the notch root, so that short crack growth rates were faster in as-broached specimens than in polished specimens. In the polished U-notch of Batch B specimens, intense slip bands developed. Cracks were observed to propagate along slip bands or along grain boundaries. Some intergranular propagation in IN718 is expected at 600^{o}C in air, because of oxidation embrittlement of grain boundaries [5,8,30]. In the Batch B U-notches, it is proposed that surface crack propagation of the crack along slip bands and grain boundaries produced a longer, more tortuous crack path, resulting in partial shielding of the crack from the applied stresses and hence a lower crack propagation rate. In Batch A specimens, removal of the broaching marks may have reduced the local crack driving force by eliminating the stress concentrating effect of the broaching marks, even though the actual crack path was unaffected. Removal of some of the surface work-hardened layer by polishing could also have acted to reduce surface crack propagation rates in Batch A.

Another difference between the two batches is the absence of slip bands on polished notch surfaces of the batch which had the deformed surface layer (Batch A). Ghonem et al. [5,33] found that pre-straining IN718 at room temperature produced more homogeneous slip during subsequent fatigue testing at 650^{o}C in air. Their observation is relevant to the case of the U-notch roots because it demonstrates that prior deformation at room temperature can influence subsequent high temperature slip behaviour. If the deformation layer in Batch A did result in more homogeneous slip at 600^{o}C, as suggested by the work of Ghonem et al. [5,34], this would explain the absence of slip bands on polished notch surfaces. We think that the reduced propensity of slip band formation is caused by the forest of dislocations introduced by room temperature deformation (by prestraining introduced by broaching with a blunt tool) interacting with moving dislocations, thus hampering deformation by long range slip over a limited set of slip planes, i.e. by dispersing slip. In the Batch A U-notch tests, surface cracks were straight and transgranular, which is also consistent with the theory of Ghonem et al. [5,34] that homogeneous slip reduces intergranular cracking. It was observed that below the notch surface, there was a transition to mixed transgranular-intergranular cracking of the material. The depth at which this occurred was 30-50 μm in the Batch A specimens, greater than the visible depth of the surface deformation layer, but perhaps at the boundary of the region of

material in which homogeneous slip was enhanced. However, reduced fatigue lives in Batch A compared to Batch B are indicative of a detrimental effect of pre-straining. Substantial work hardening will also have reduced the ductility of the material within the deformation layer, possibly reducing its resistance to crack initiation and propagation.

VI CONCLUSIONS

The fatigue behaviour of IN718 U-notch specimens was found to be different in two batches of specimens which had similar microstructures in terms of grain size, primary carbide content and the presence of grain boundary δ phase. However, Batch A specimens were found to have a work-hardened deformation layer in the broached notch, and a lower notch surface roughness than Batch B. Batch B specimens exhibited substantially longer fatigue lifetimes than Batch A under the same experimental conditions. It has been shown that an increase in yield stress in the Batch A deformation layer could account for the difference in strain-life behaviour between the two batches. Fatigue lifetimes were affected by notch surface roughness. Polishing the notch had a beneficial effect on fatigue life in both batches.

For Batch A specimens, it was the oxidised sub-surface carbides, rather than oxide eruptions in general, that were the more numerous type of crack initiation site in U-notch specimens tested in air. For Batch B specimens, initiation at oxidised sub-surface carbides was infrequent and fewer initiation sites were observed under the same conditions, despite the rougher notch surface. The deformation layer in Batch A affected crack initiation and propagation behaviour, possibly by influencing the degree of slip homogeneity. Slip bands were not observed on the surface of polished notches in Batch A, but were in Batch B, suggesting more heterogeneous slip in Batch B.

Crack initiation kinetics varied with applied stress. At the lower stress levels of σ_{max} = 750 MPa or 790 MPa in Batch A, there was an initial incubation period at the start in which no cracks were observed. Following the initially slow rate of crack initiation, there was a transition to behaviour in which the number of cracks appearing increased at a steady rate. The factors controlling this rate are thought to be the time required for oxidation of carbides in different parts of the specimen and the time required for accumulation of sufficient cyclic damage in the material to initiate further cracks. The number of cracks initiated eventually reached a plateau, attributed to a combination of exhaustion of potential crack initiation sites, reduction in the local strain at initiation sites due to shielding by neighbouring cracks, and crack coalescence. At σ_{max} = 885 MPa in Batch B specimens, fatigue failure was controlled by initiation and growth of a single crack, with most of the other cracks initiating in the stress-strain field ahead of the tip of the growing crack or in the residual ligaments. One possible

cause of the difference between Batch A and Batch B tests was the much higher stress level used for Batch B. This led to a shorter fatigue life, allowing less time for initiation by primary carbide oxidation.

In polished notch roots, the surface cracks in Batch A were all remarkably straight, with no deflections except those occurring during crack coalescence. This may be related to the deformation layer observed in the Batch A notch roots. Slip bands were observed on the Batch B polished notch surface, but not in the equivalent tests performed in Batch A. The absence of slip bands in Batch A may have been due to extensive work hardening in the surface deformation layer, which prevented easy dislocation glide and the formation of slip bands.

ACKNOWLEDGEMENTS

This work was funded by the United Kingdom Engineering and Physical Sciences Research Council and ALSTOM Power. The authors wish to thank Dr. R. Jakeman, Dr. S. J. Moss and M. Hughes of ALSTOM Power for valuable technical discussions and provision of the IN718 material.

FIGURES

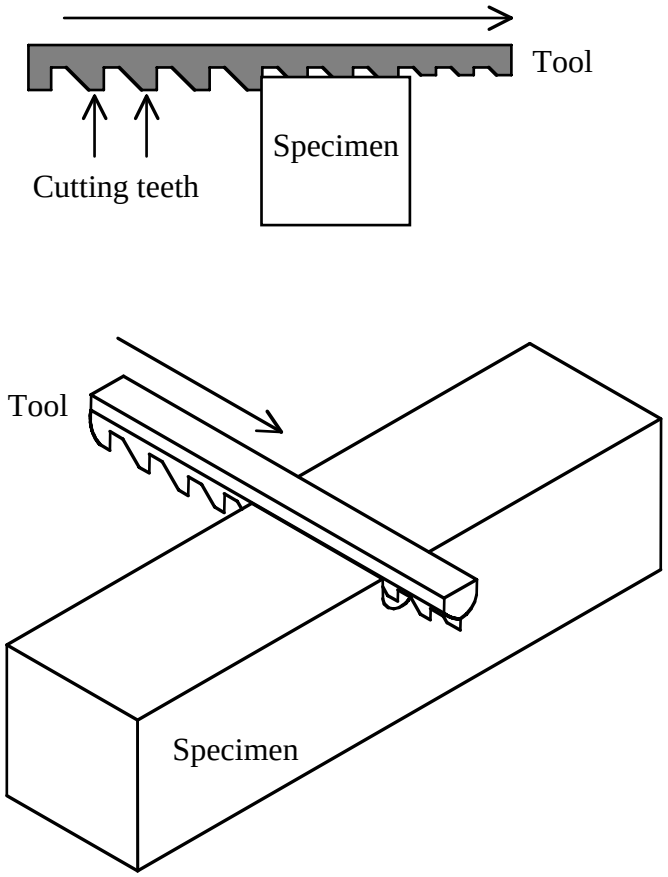

Figure 1: Schematic diagram of the broaching process used to produce the U-notches. A similar process is used for the fir tree root fixings in gas turbine disc rims.

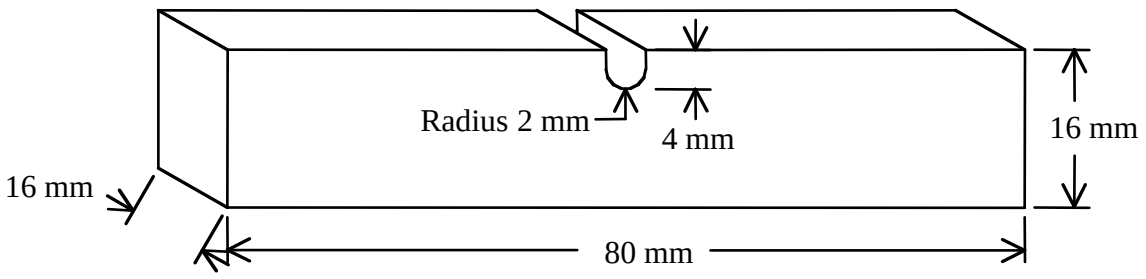

Figure 2: U-notch specimen geometry.

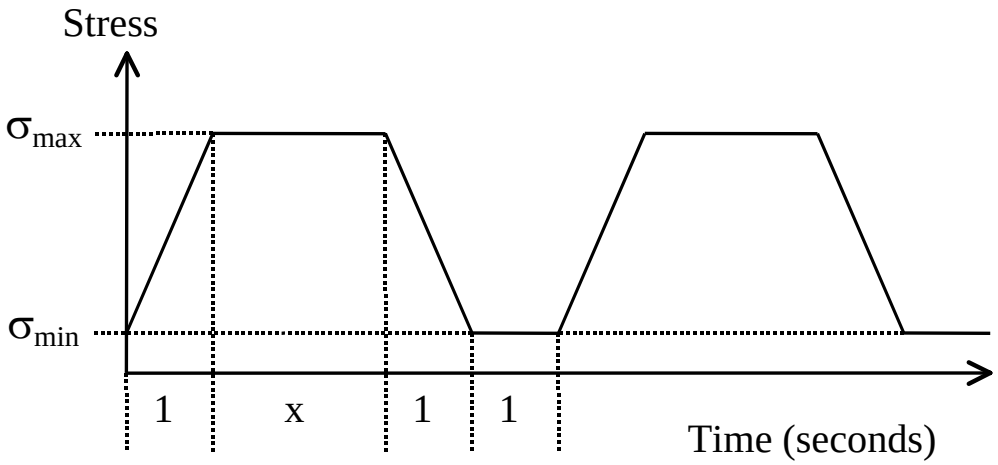

Figure 3: Trapezoidal waveform (1-x-1-1) used in fatigue testing, where x = dwell in seconds at maximum load. For all tests x=1.

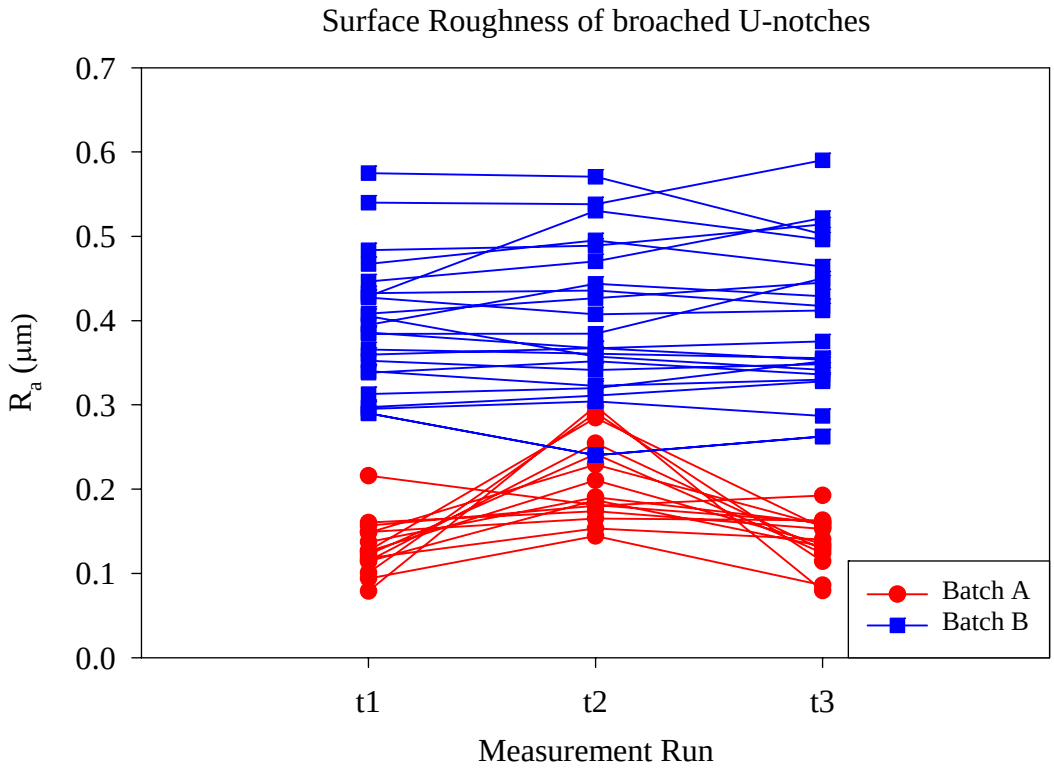

Figure 4: Surface roughness measurements in U-notch roots. Values of R_a for Batch A and Batch B.

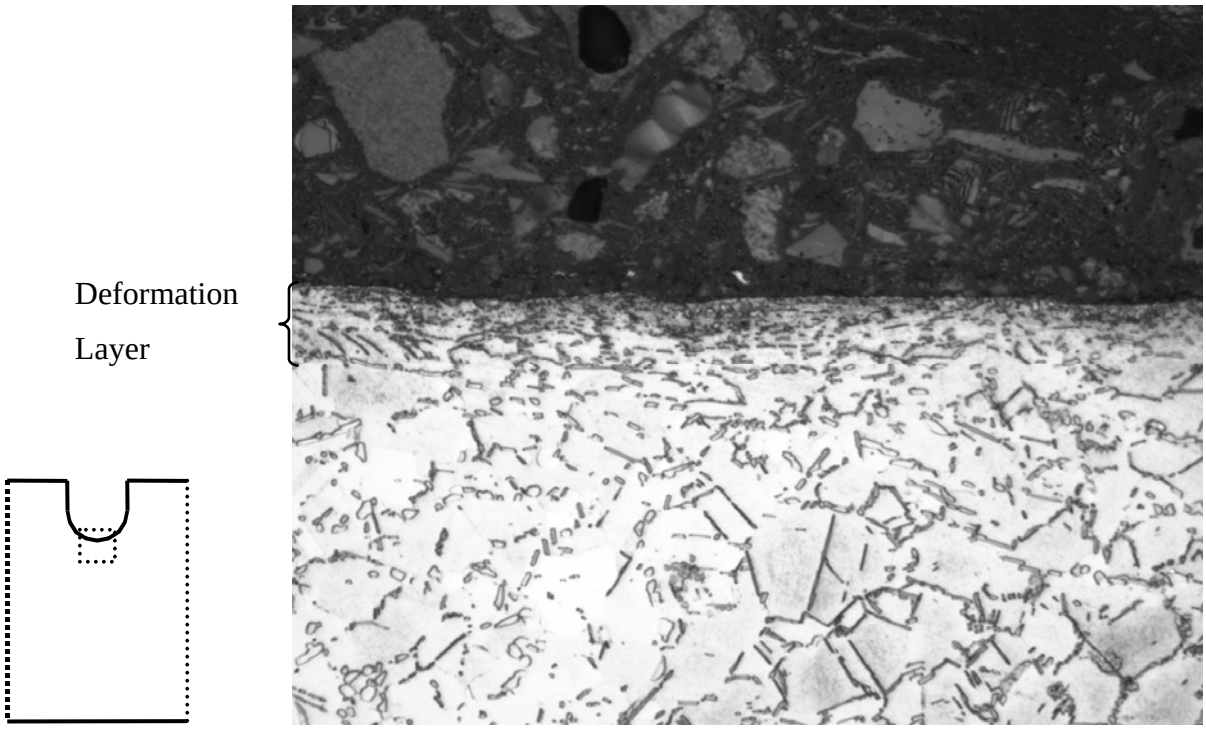

(a)

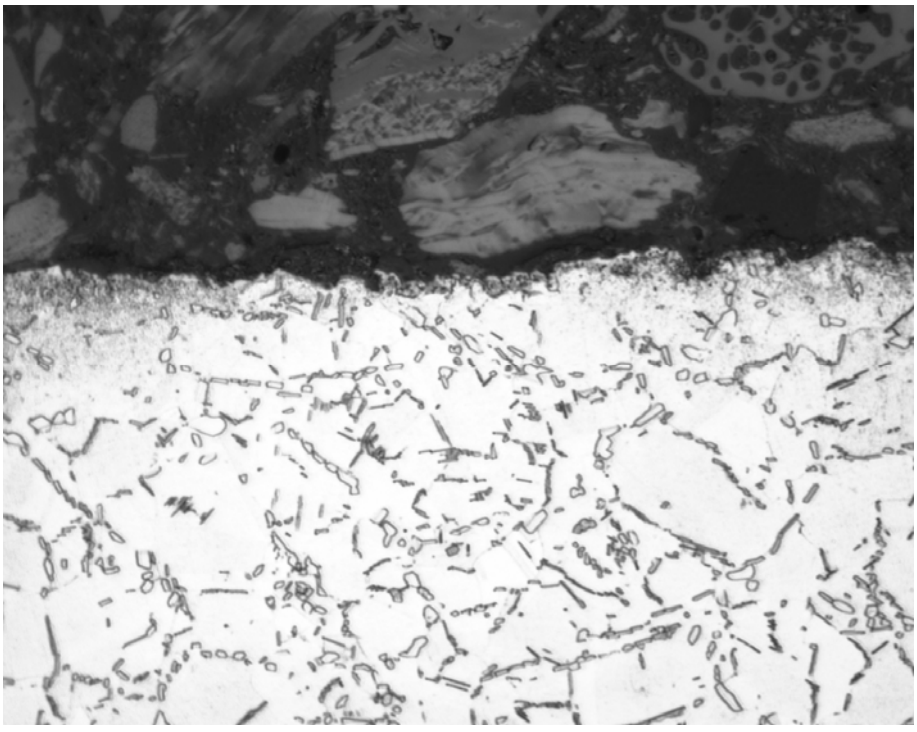

(b)

Figure 5: Optical micrographs of sections through U-notch root. (a) Batch A specimen, showing presence of a deformation layer at the surface. (b) Batch B specimen, with no deformation layer in the notch root. The higher surface roughness of the Batch B specimen can be seen.

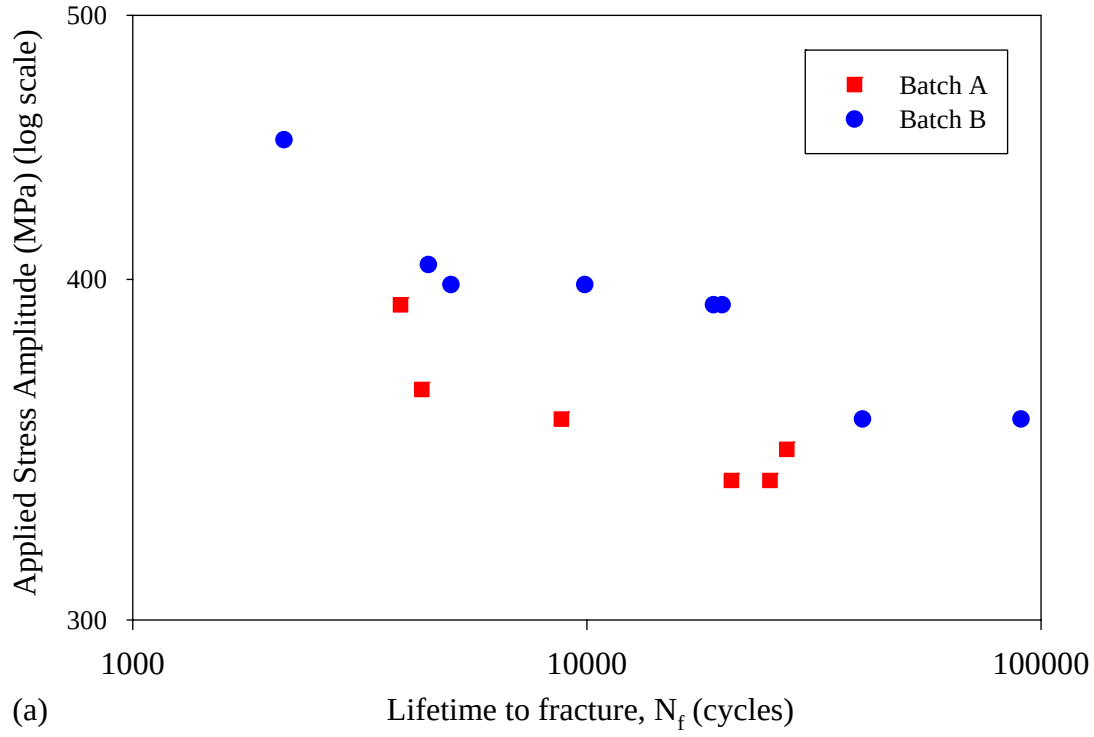

(a)

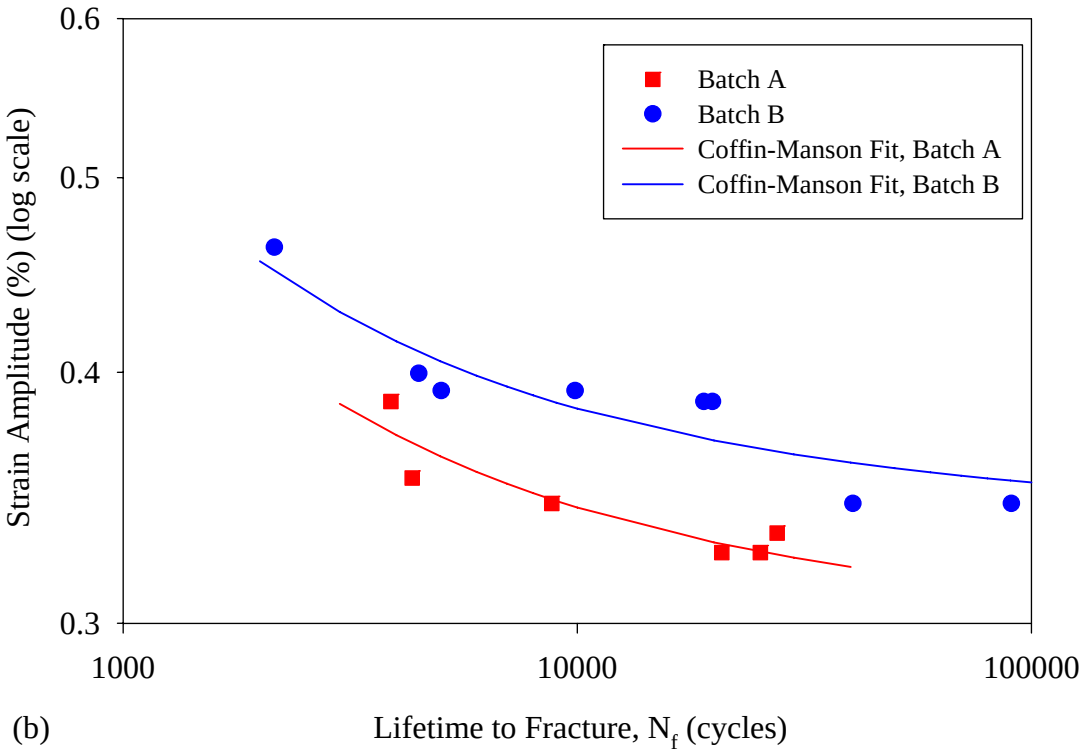

(b)

Figure 6: Stress and strain-life curves for as-broached U-notch specimens (1-1-1-1 trapezoidal waveform, 600°C, in air).

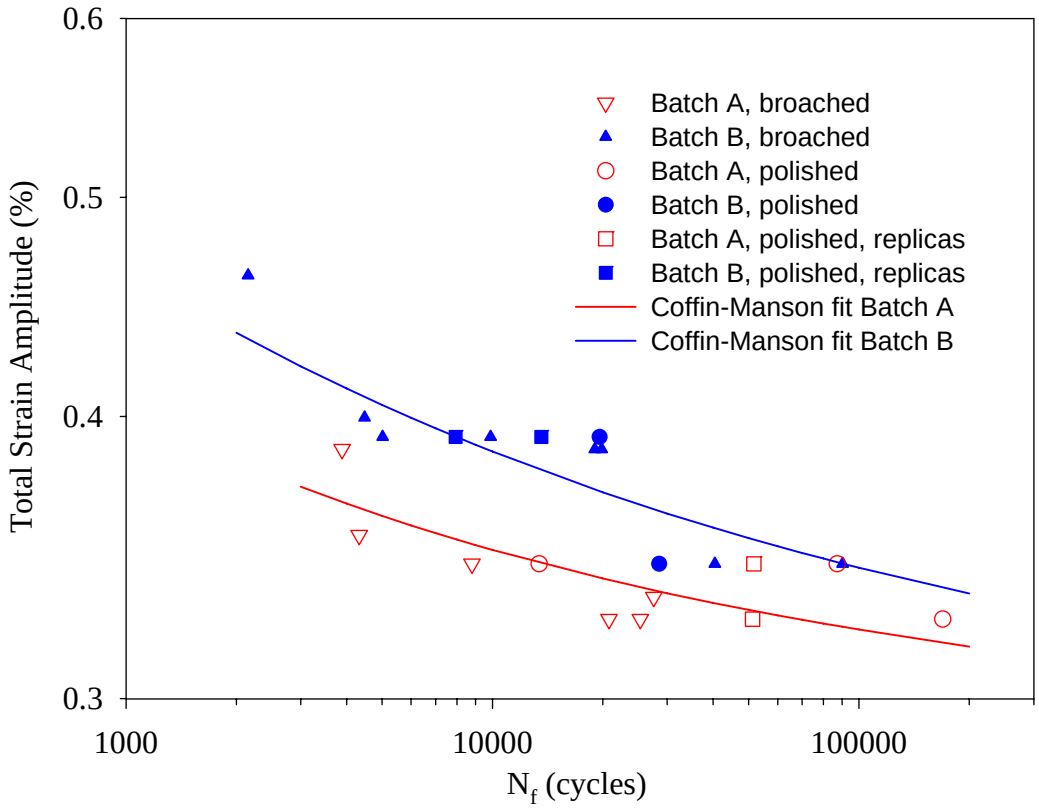

Figure 7: Strain-life data for all U-notch tests performed at 600°C, using a 1-1-1-1 trapezoidal waveform. The data is fitted with Coffin-Manson type expressions for strain-life data.

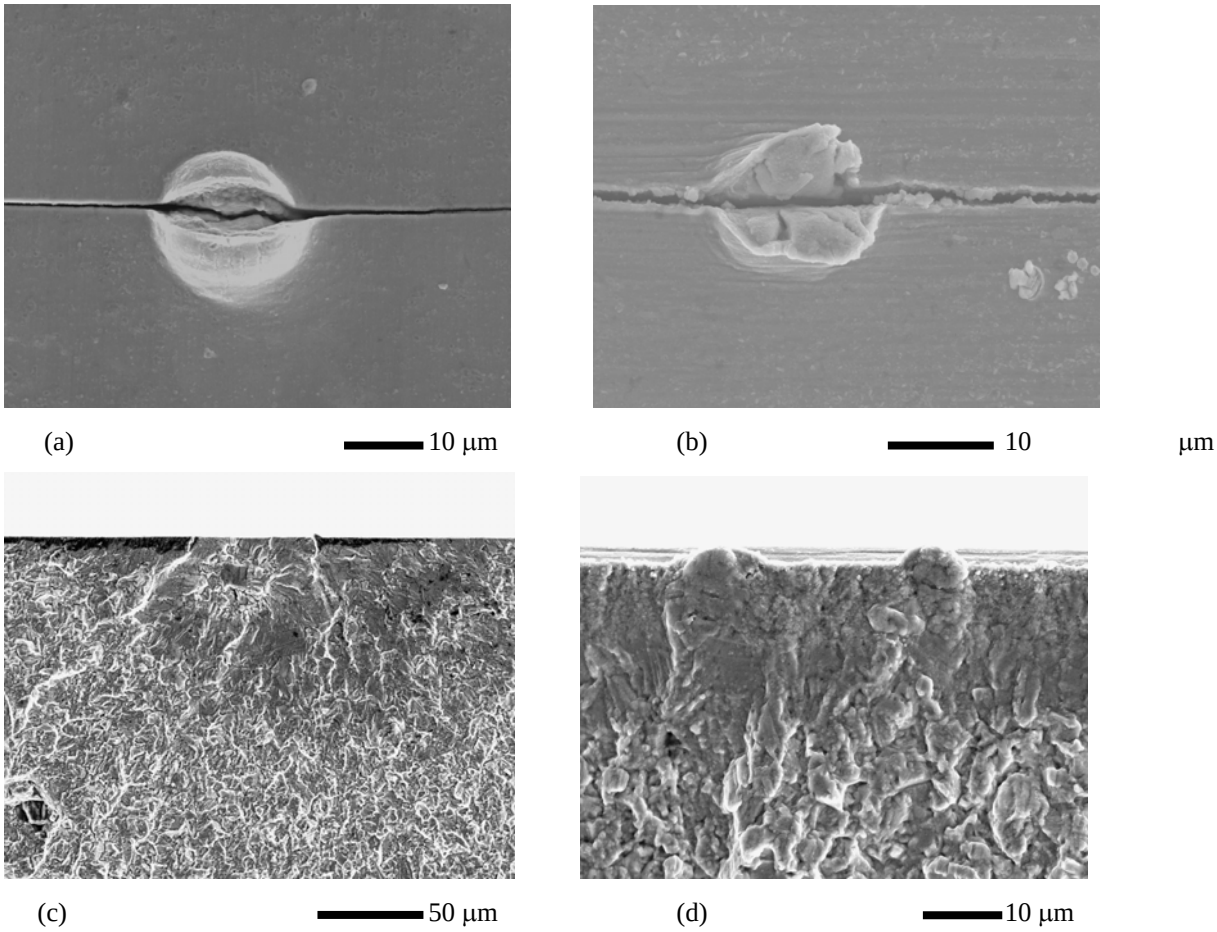

Figure 8: Examples of short crack initiation sites observed in the notch root of Batch A and Batch B specimens tested in air. (a) shows a crack initiated from a bulged site, commonly seen in the notch root in Batch A (b) shows a surface eruption, with some deformation visible initiating a crack also in Batch A. (c) Initiation in Batch B at a sub-surface (Ti,Nb)N particle (rectangular shaped particle about 15μm below surface). (d) Small bulge-like features, but NOT associated with an oxidised (Nb,Ti)C particle (SEM, SEI).

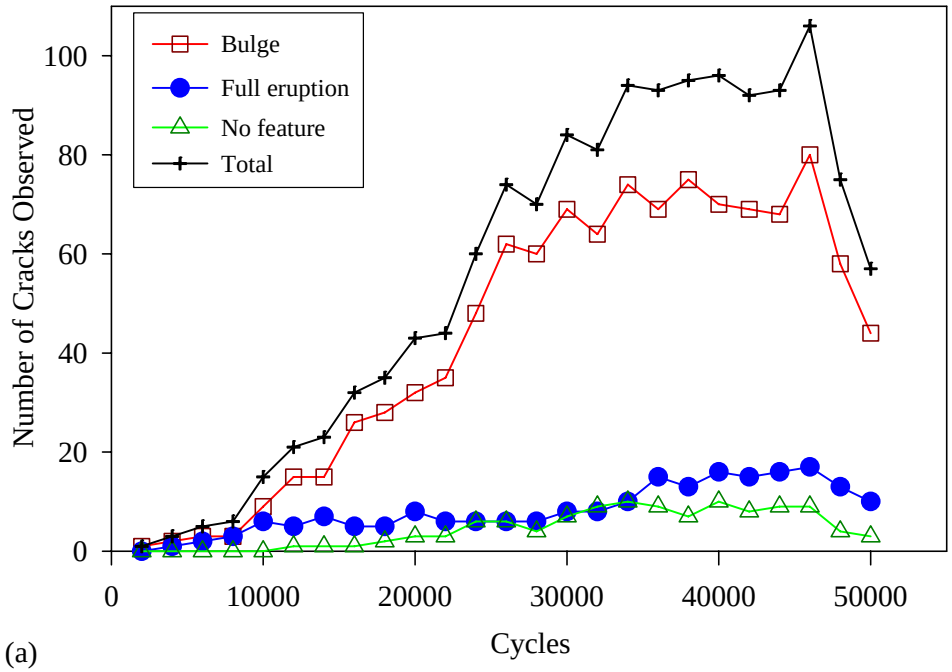

(a)

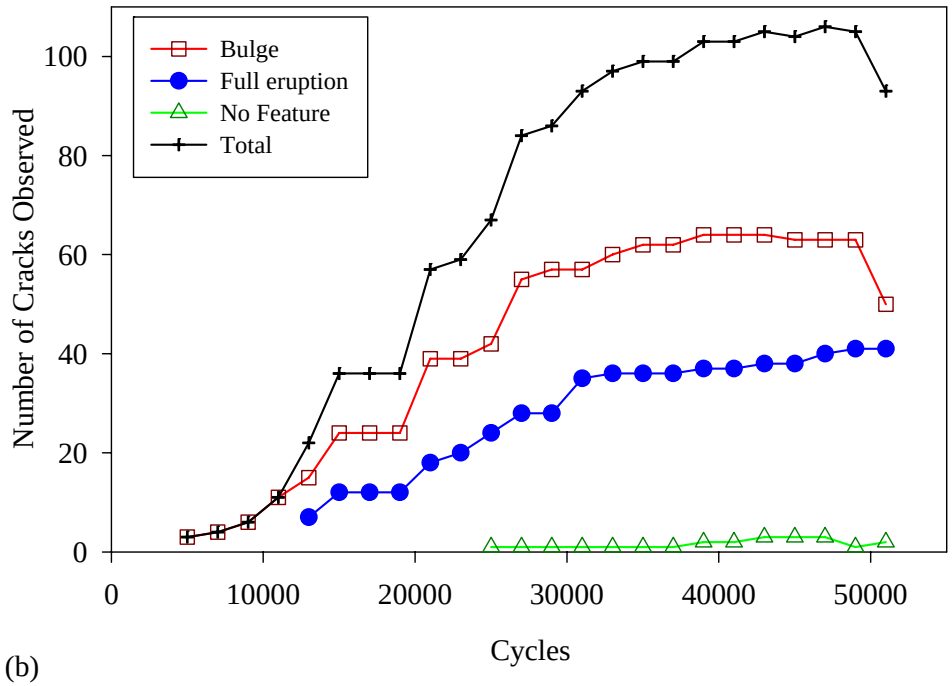

(b)

Figure 9: Quantification of number of cracks observed on replicas from polished Batch A U-notch specimens (trapezoidal waveform 1-1-1-1, 600°C, in air): (a) σ_{max} = 750 MPa; (b) σ_{max} = 790 MPa.

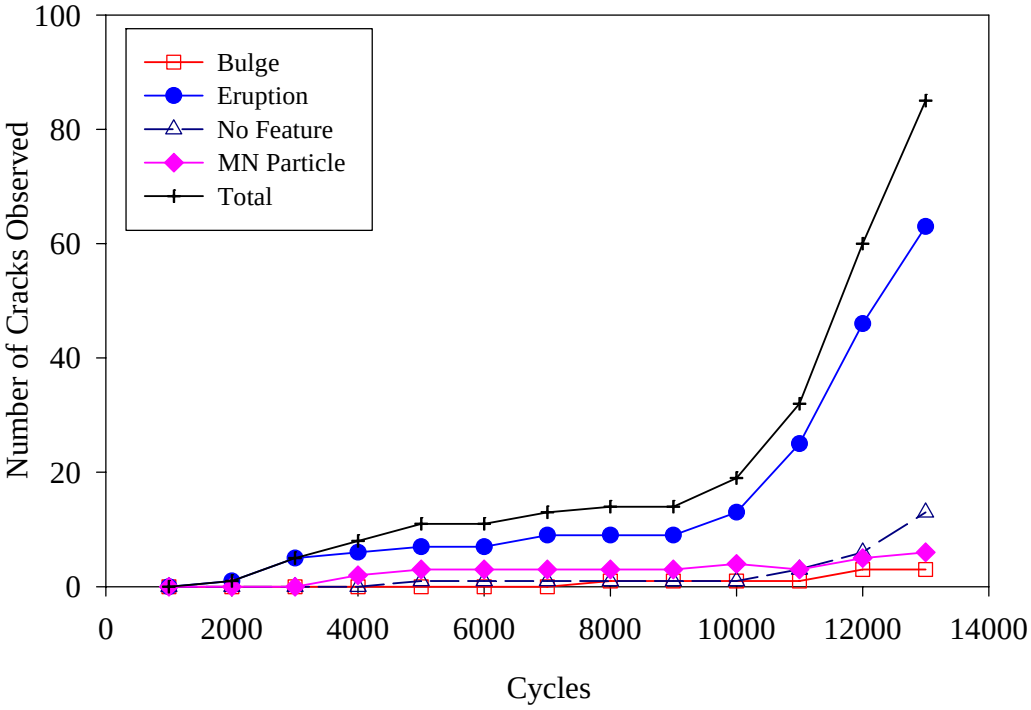

(a)

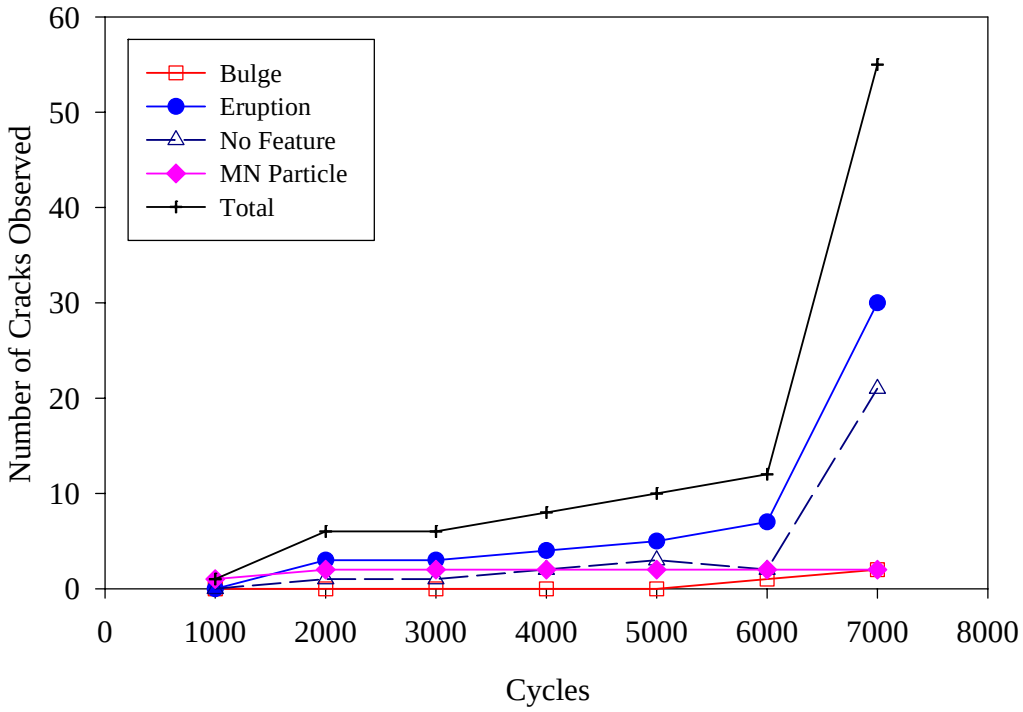

(b)

Figure 10: Quantification of number of cracks observed on replicas from polished Batch B U-notch specimens (trapezoidal waveform 1-1-1-1, 600°C, in air) σ_{max} = 885 MPa: (a) test 1 (b) test 2.

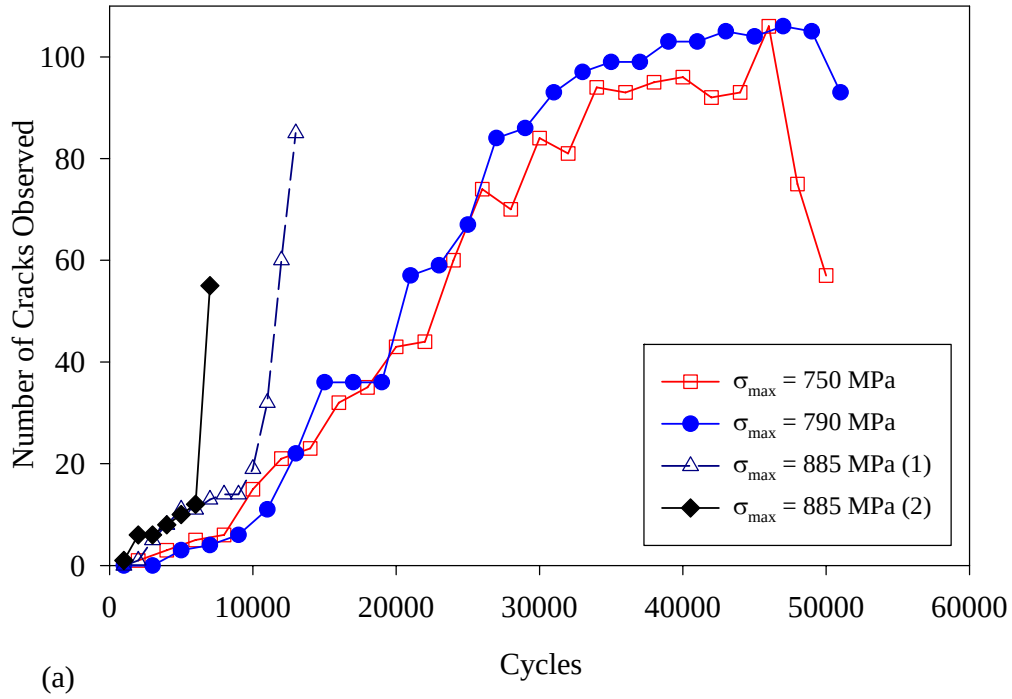

(a)

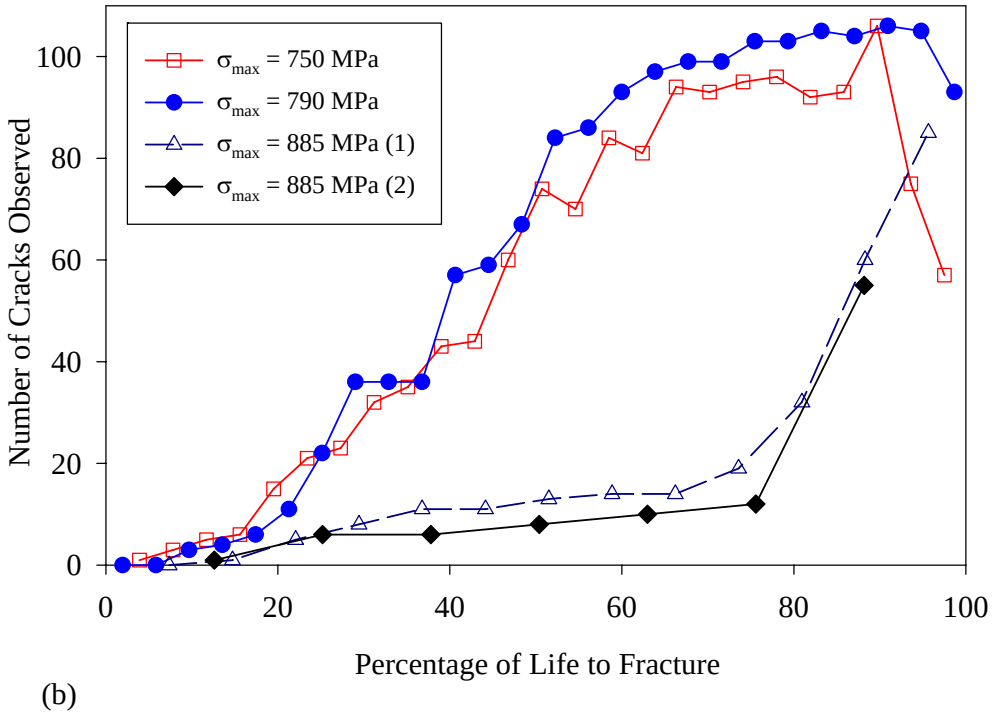

(b)

Figure 11: Comparison of crack initiation behaviour for tests on polished U-notch specimens at different stress levels. (a) in terms of cycles; (b) in terms of percentage of life to fracture. The higher stress level data (885MPa) is from batch B samples, and the 2 lower stress levels are data from Batch A samples.

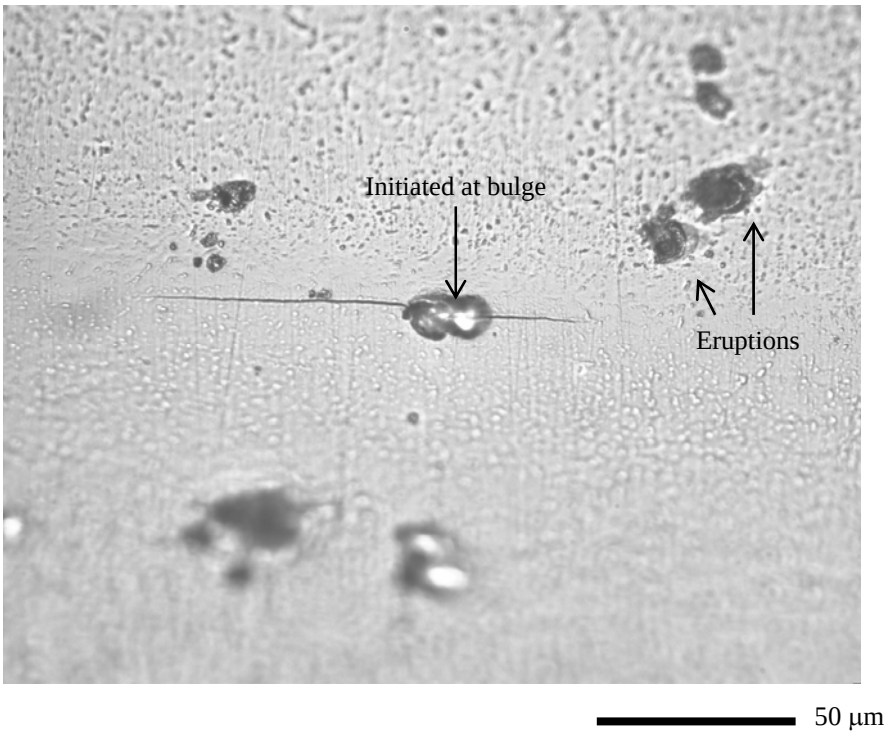

Figure 12: Crack A from test A600-790-1-PR-01 after 15000 cycles (σ_{max} = 790 MPa, Batch A), showing asymmetry about the initiation point. (Optical microscopy from acetate replica).

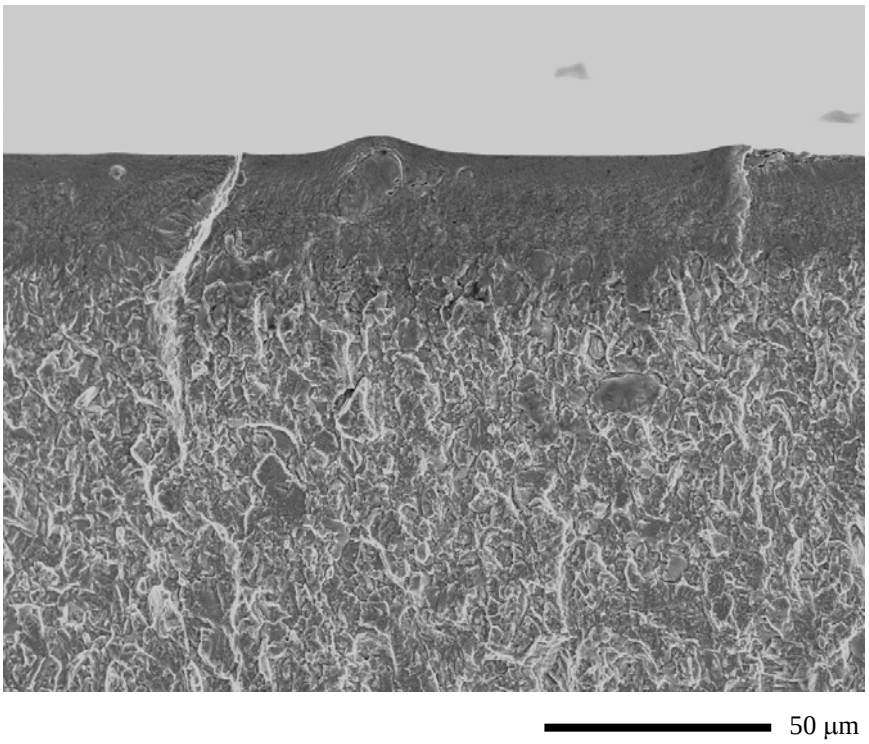

Figure 13: SEM image of fracture surface showing transition from very flat, transgranular fracture to mixed transgranular-intergranular fracture in Batch A specimen. Note the bulge above the (Nb,Ti)C particle at the crack initiation site.

Figure 14: Crack Y from test B600-885-1-PR-02 after 4000 cycles (σ_{max} = 885 MPa, Batch B), showing crack deflections. Crack propagation appeared to be mixed transgranular-intergranular. (Optical microscopy from acetate replica).

(a) 100 μm

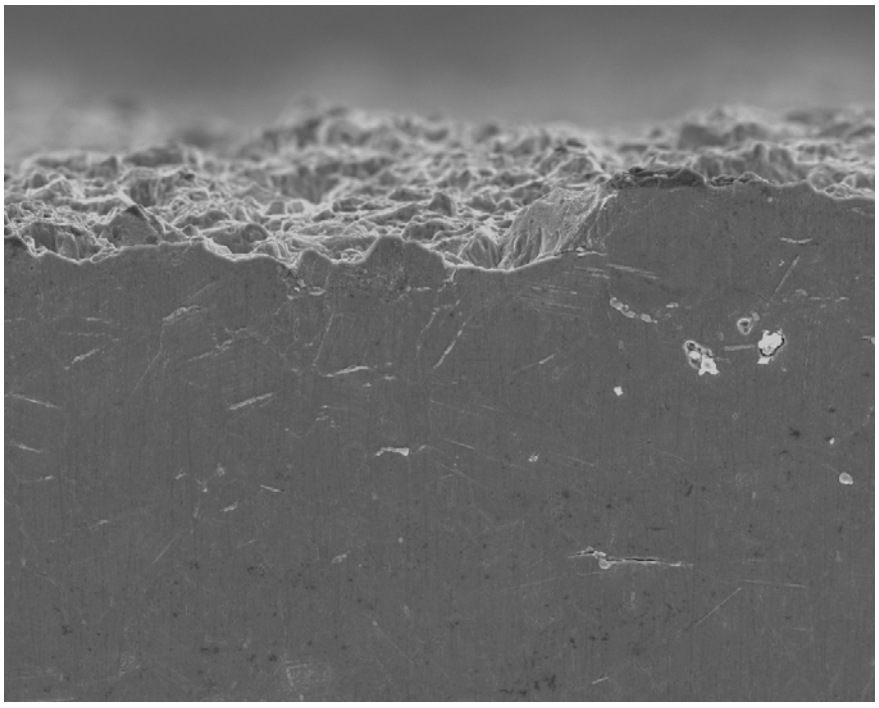

(b) 100 μm

Figure 15: Comparison of surface crack fracture paths in notch root of Batch B specimens at σ_{max} = 885 MPa. Batch B specimens. (a) as-broached; (b) polished. (SEM, SEI).

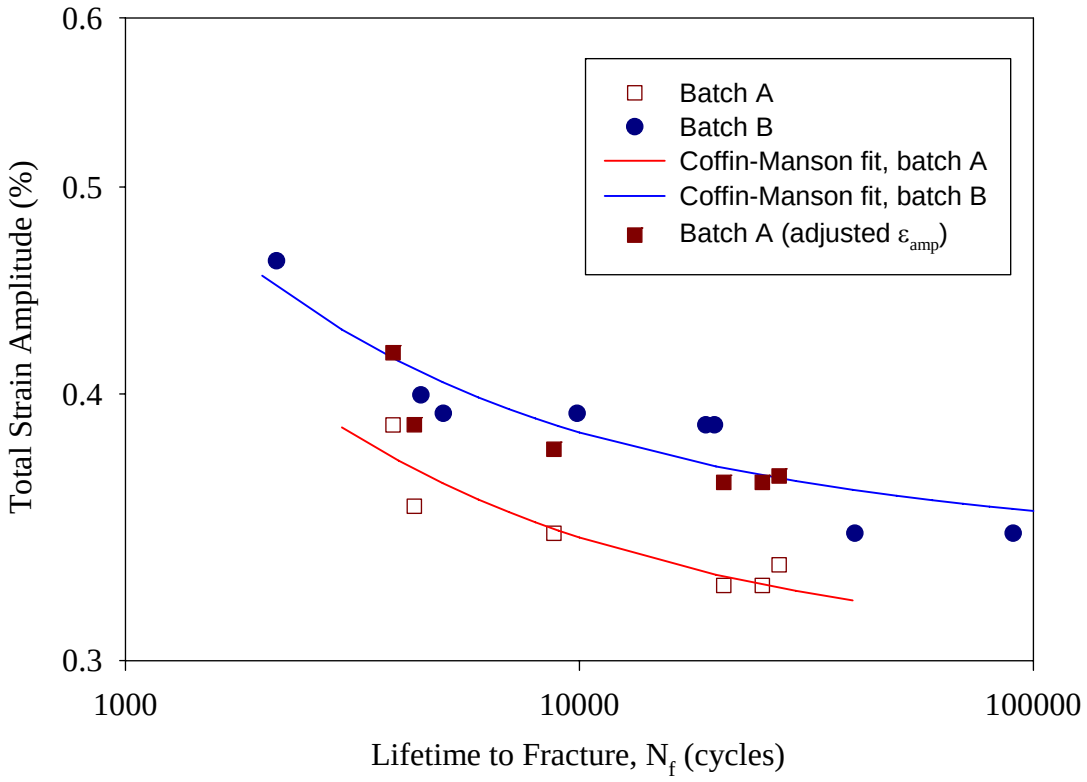

Figure 16: Modified Batch A strain-life curve for as-broached U-notch specimens, waveform 1-1-1-1, 600°C, air.

REFERENCES

[1] ASM Handbook, Machining, 10th ed., vol. 16, ASM International, Metals Park, Ohio, USA, 1995, pp. 194-211

[2] S. P. Lynch, T. C. Radtke, B. J. Wicks and R. T. Byrnes, Fatigue Fract. Engng. Mater. Struct., 1994, vol.17, pp 313-325

[3] A. Andrieu, R. Molins, H. Ghonem and A. Pineau, Mater. Sci. Engng., 1992, vol. A154, pp 21-28

[4] E. Andrieu, G. Hochstetter, R. Molins and A. Pineau, Proc. 3rd Int. Symp. Superalloys 718, 625, 706 and Various Derivatives, TMS, Warrendale, PA, USA, 1994, pp. 619-630

[5] H. Ghonem and D. Zheng, Metall. Trans., 1992, vol. 23A, pp 3067-3072

[6] P. Shahinian and K. Sadananda, Trans. ASME J. Engng. Mater. Tech., 1979, vol. 101, pp 24-230

[7] H. Ghonem, T. Nicholas and A. Pineau, Fatigue Fract. Engng. Mater. Struct., 1993, vol. 16, pp 565-576

[8] H. Ghonem, T. Nicholas and A. Pineau, Fatigue Fract. Engng. Mater. Struct., 1993, vol. 16, pp 577-590

[9] J. P. Pedron and A. Pineau, Mater. Sci. Engng., 1982, vol. 56, pp 143-156

[10] E. Andrieu, R. Cozar and A. Pineau, Proc. Superalloy 718 - Metallurgy & Applications, TMS, Warrendale PA, USA, 1989, pp. 241-247

[11] L. A. James, Engng. Fract. Mech., 1986, vol. 25, pp 305-314
[12] M. R. Bache, W. J. Evans and M. C. Hardy, Int. J. Fatigue, 1999, vol. 21 Supp., S69-S77
[13] D. Fournier and A. Pineau, Metall. Trans., 1977, vol. 8A, pp. 1095-1105
[14] J. C. Healy, L. Grabowski and C. J. Beevers, Int. J. Fatigue, 1991, vol. 13, pp. 133-138
[15] T. Denda, P. L. Bretz and J. K. Tien, Metall. Trans., 1992, vol. 23A, pp 519-526
[16] G. R. Leverant and M. Gell, Trans. Metall. Soc. of AIME, 1969, vol. 245, p.1167
[17] J. Reuchet and L. Remy, Mater. Sci. Engng., 1983, vol. 58, pp 19-32
[18] J. Reuchet and L. Remy, Mater. Sci. Engng., 1983, vol. 58, pp 33-42
[19] M. Reger and L. Remy, Mater. Sci. Engng., 1988, vol. A101, pp 47-54
[20] M. Reger and L. Remy, Mater. Sci. Engng., 1988, vol. A101, pp 55-63
[21] G. Sjoberg, N-G. Ingesten and R. G. Carlson, in Proc. 2nd Int. Symp. Superalloy 718, 625 & Various Derivatives, TMS, Warrendale, PA, USA, 1991, p. 603
[22] P. A. S. Reed, F. Hachette, D. Thakar, T. Connolley and M. J. Starink, in Proc. 8th Int. Conf. Mechanical Behaviour of Materials (ICM8), F. Ellyin and J.W. Provan (Eds), Fleming Printing Ltd. Victoria, BC, Canada, 1999, vol. 1, pp. 418-423
[23] T. Connolley, P. A. S. Reed and M. J. Starink, in Proc. 5th Charles Parsons Turbine Conference, Institute of Materials, London, 2000, pp. 982-998
[24] T. Connolley, M. J. Starink and P. A. S. Reed, in Proc. 9th International Symposium on Superalloys, T.M. Pollock, R.D. Kissinger, R.R. Bowman, K.A. Green, M. McLean, S. Olson and J.J. Scirra (Eds), TMS, Warrendale, PA, USA, 2000, pp. 435-444
[25] T. Connolley, P. A. S. Reed and M. J. Starink, Mater. Sci Engng, 2003, vol. A340, pp 130-145
[26] T. Connolley, PhD thesis, University of Southampton, 2001
[27] H. F. Merrick, Metall. Trans., 1974, vol. 5, pp.891-897
[28] J. B. Clark and A. J. McEvily, Acta Met., 1964, vol. 12, pp. 1359-1372
[29] S. Floreen and R. H. Kane, Fat. Engng. Mater. Struct., 1980, vol. 2, pp. 401-412
[30] R. G. Andrews, A. K. Koul and P. Au, Proc. 2nd Int. Symp. Superalloy 718, 625 & Various Derivatives, Ed. Loria E. A., TMS, Warrendale PA, USA, 1991, pp.943-954
[31] J. R. Cahoon, W. H. Broughton and A. R. Kutzak, Metall. Trans., 1971, vol. 2, pp. 1979-1983
[32] Z. Mei, C. R. Krenn and J. W. Morris, Metall. & Mater. Trans. A, 1995, vol. 26A, pp.2063-2073
[33] D. Zheng, A. Rosenberger and H. Ghonem, Mater. Sci. Engng., 1993, vol. A161, pp. 13-21